UNIVERSITY OF CALIFORNIA SAN DIEGO

Non-Boussinesq stability analysis of natural convection over a horizontal hot plate

A thesis submitted in partial satisfaction
of the requirements for the degree of Master of Science

in

Engineering Sciences (Aerospace Engineering)

by

Haotian Sun

Committee in charge:

Professor Antonio L. Sánchez, Chair
Professor Eugene R. Pawlak
Professor Stefan Llewellyn Smith

2018

The Thesis of Haotian Sun is approved, and it is acceptable in quality and form for publication on microfilm and electronically:

Chair

University of California San Diego

2018

Table of Contents

List of Figures

ABSTRACT OF THE THESIS

Non-Boussinesq stability analysis of natural convection over a horizontal hot plate

by

Haotian Sun

Master of Science in Engineering Sciences (Aerospace Engineering)

University of California San Diego, 2018

Professor Antonio L. Sánchez, Chair

Flow that develops over a semi-infinite horizontal plate has been studied over the past decades. In this particular case, a boundary-layer flow over a horizontal hot plate is chosen and its stability characteristics at a finite distance from the leading edge are analyzed. A critical value of the Grashof number Gr based on the local boundary-layer thickness is defined and used to analyze the resulting instability.

Due to the nature of the hot plate, the Boussinesq approximation used in previous linear stability analyses becomes less desirable since wall-to-ambient temperature differences are not

close to unity. And as a result, a non-Boussinesq analysis is needed and presented here for two instability modes: vortex, i.e. Görtler-like streamwise vortices, and wave, i.e. spanwise traveling waves.

Numerical results are presented such as the neutral stability curve, and critical Grashof number for Prandtl numbers of 0.7 over a wide range of wall-to-ambient temperature ratios. It is found that as this ratio increases, the susceptibility of the flow to the vortex mode of instability decreases while the wave mode instability becomes more prominent. The present study provides an approach suitable for both the vortex and wave instability modes with different wall-to-ambient temperature ratio. The results for the two modes are compared with each other as well as to other available instability data.

1 Introduction

Flow that develops over a semi-infinite plates is one of the fundamental problems that appears in many science and engineering applications. Ever since the beginning of the 20th century, research has been performed on this topic. However, the majority of the studies available in the literature have focused on experiments, by using air or water as working fluid. In fact, at the time, numerical methods for the solution of the governing equations were not yet fully developed and valid [1].

Schmidt and Beckmann [2] first studied free convection over a horizontal flat surface experimentally in the 30s. Sparrow and Husar [3] were the first to identify the stability issue experimentally for an inclined plate. Two modes of instability were discovered. Vortex instability represents the stability mode involving streamwise Görtler-like vortices, whereas wave instability represents that involving spanwise traveling waves following existing terminology [4] [5] from here on.

With the help of more advanced analytical and numerical approaches, a large body of theoretical efforts was obtained. However, most of them were performed in the Boussinesq approximation, when the wall-to-ambient temperature ratio is close to 1.

The present investigation focus on the analysis of vortex and wave instability of a boundary-layer natural convective flow over a horizontal, upward-facing hot plate for various wall-to-ambient temperature ratios. Unlike the previous analyses, it does not employ the Boussinesq approximation or study an inclined plate [6]. The present study covers a temperature ratio ranging up to 2.55 in which no available stability results have been reported in existing literature. A local stability analysis using normal mode is employed by our work. A unique neutral curve in the Grashof—wave number plane can be established for each mode. In reality, the mode with the lowest associated critical Grashof number for all wave numbers would dominate.

The thesis is structured as follows. Section 2 presents the governing equations and boundary conditions for the base flow and for the linear stability analysis. Section 3 and 4 study the vortex and wave instability, respectively. Analysis and comparison are made to the two modes in

Section 5 while Section 6 concludes.

2 Problem formulation

The problem considered here is shown schematically in Fig. 1:

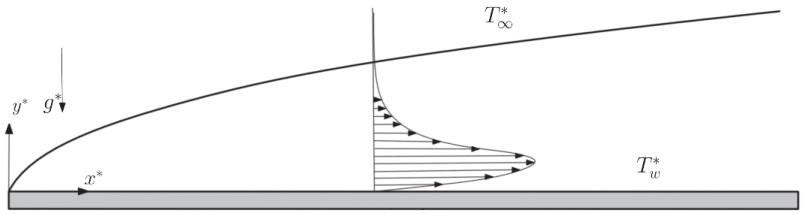

Figure 1: Schematic diagram of the boundary-layer flow over a hot horizontal surface [6].

The temperature of the horizontal upward-facing plate is held at a constant value ${T_w}^*$ which is higher than the ambient temperature ${T_\infty}^*$ found in the surrounding quiescent air atmosphere. The conservation equations can be written in the following form,

$$\frac{\partial \rho^*}{\partial t^*} + \nabla^* \cdot (\rho^* \mathbf{v}^*) = 0 \tag{1}$$

$$\rho^* \frac{\partial \mathbf{v}^*}{\partial t^*} + \rho^* \mathbf{v}^* \cdot \nabla^* \mathbf{v}^* = -\nabla^* p^* + (\rho^* - \rho_\infty^*)\mathbf{g}^* + \nabla^* \cdot [\mu^* (\nabla^* \mathbf{v}^* + \nabla^* {\mathbf{v}^*}^T] \tag{2}$$

$$\rho^* \frac{\partial T^*}{\partial t^*} + \rho^* \mathbf{v}^* \cdot \nabla^* T^* = \frac{1}{Pr} \nabla^* \cdot [\mu^* \nabla^* T^*] \tag{3}$$

with the following boundary conditions:

$$u^* = v^* = w^* = T^* - T_w^* = 0 \qquad \text{at } y^* = 0 \text{ and } x^* > 0 \tag{4}$$

$$u^* = v^* = w^* = T^* - T_\infty^* = p^* = 0 \qquad \text{as } ({x^*}^2 + {y^*}^2) \to \infty \text{ and } x^* > 0$$

The asterisk in the text indicates the corresponding quantity is dimensional while $\rho^*, \mathbf{v}^*$ and T^* represent the density, velocity, and temperature of the gas, respectively. The velocity components $\mathbf{v}^* = (u^*, v^*, w^*)$ correspond to the streamwise distance measured along the plate from the leading

edge x^*, the transverse distance from the surface of the plate y^* and the spanwise coordinate z^* in the cartesian coordinates. Gravity becomes $\mathbf{g}^* = -g^*\mathbf{e_y}$.

The following equations of state are then needed along with the Prandtl number and ambient kinematic viscosity. The ∞ subscript denotes properties in the ambient air.

$$R = \frac{\rho^*}{\rho^*_\infty} = \frac{T^*_\infty}{T^*} \tag{5}$$

$$\frac{\mu^*}{\mu^*_\infty} = \frac{\kappa^*}{\kappa^*_\infty} = (\frac{T^*}{T^*_\infty})^\sigma \tag{6}$$

$$Pr = \frac{c^*_p \mu^*_\infty}{\kappa^*_\infty} \tag{7}$$

$$\nu^*_\infty = \frac{\mu^*_\infty}{\rho^*_\infty} \tag{8}$$

With air as the working fluid, a Pr value of 0.7 and a σ value of 2/3 are chosen. The present flow begins as a Navier-Stokes flow from its leading edge with its characteristic properties defined as the following. Their derivations are based on the assumption that in this region, x^* and y^* are of the same order of magnitude. However, in our case, an assumption that the appearance of instability happens much further downstream is made and only the boundray-layer region is studied.

$$x^*_{NS} = y^*_{NS} = (\frac{{\nu^*_\infty}^2}{g^*})^{\frac{1}{3}} \tag{9}$$

$$u^*_{NS} = (\nu^*_\infty g^*)^{\frac{1}{3}} \tag{10}$$

Such assumption implies with our definition of Gr, shown in Eq. (9), the appearance of the instability occurs when the critical value of Gr is much larger than 1. This is required to enable us to use the conditions of the nearly parallel approximation, with the self-similar boundary layer solutions used to evaluate the base flow, as indicated below. Hence the streamwise velocity u^*,

transverse velocity v^* and streamwise velocity ${u_0}^*$ at $x^* = {x_0}^*$ take the form,

$$u^* = ({g^*}^2 \nu_\infty^* x^*)^{\frac{1}{5}} \tag{11}$$

$$v^* = (\frac{g^* {\nu_\infty^*}^3}{{x^*}^2})^{\frac{1}{5}} \tag{12}$$

$$u_0^* = ({g^*}^2 \nu_\infty^* x_0^*)^{\frac{1}{5}} \tag{13}$$

while the boundary layer thickness being y^* with δ_0 representing the local one at $x^* = {x_0}^*$,

$$y^* = (\frac{{\nu_\infty^*}^2 {x^*}^2}{g^*})^{\frac{1}{5}} \tag{14}$$

$$\delta_0^* = (\frac{{\nu_\infty^*}^2 {x_0^*}^2}{g^*})^{\frac{1}{5}} \tag{15}$$

The value of the associated Grashof number then determines the stability of the boundary layer at a given streamwise location $x^* = {x_0}^*$. A different approach to define the Grashof number is taken from [7] [8]. In our case, Gr is in fact the Reynolds number based on the local values of the thickness δ_0 and streamwise velocity ${u_0}^*$.

$$Re = \frac{VD}{\nu} = \frac{u_0^* \delta_0^*}{\nu} = Gr = \frac{x_0^*}{\delta_0^*} = (\frac{{x_0^*}^3 g^*}{{\nu_\infty^*}^2})^{\frac{1}{5}} = \frac{{\delta_0^*}^{\frac{3}{2}} {g^*}^{\frac{1}{2}}}{\nu_\infty^*} \tag{16}$$

2.1 Base flow

The base flow is needed for the following stability analysis. In order to do so, we obtain the steady solution. Clarke and Riley [9] showed that the resulting solution is self-similar. The velocity field will be represented in terms of the stream function ψ^* and the boundary-layer region characteristic thickness will be scaled dimensionlessly as η from the previous equations, Eq. (11)-Eq. (15). A prime is used to denote differentiation with respect to η:

$$\eta = \frac{y^*}{({\nu_\infty^*}^2 {x^*}^2 {g^*}^{-1})^{\frac{1}{5}}} \tag{17}$$

Stream function:

$$\psi^* = (g^* {\nu^*_\infty}^3 x^{*3})^{\frac{1}{5}} F(\eta), \tag{18}$$

The mass-weighted velocity field:

$$\rho^* u^* = \rho^*_\infty (g^{*2} \nu^*_\infty x^*)^{\frac{1}{5}} F' \tag{19}$$

$$\rho^* v^* = \rho^*_\infty (\frac{g^* {\nu^*_\infty}^3}{x^{*2}})^{\frac{1}{5}} (\frac{2}{5}\eta F' - \frac{3}{5}F). \tag{20}$$

The pressure and temperature functions,

$$T^* = T^*_\infty \Theta(\eta), \tag{21}$$

$$p^* = \rho^*_\infty (g^{*2} \nu^*_\infty x^*)^{\frac{2}{5}} G(\eta), \tag{22}$$

with $\Theta(\eta)$ and $G(\eta)$ being the self-similar variables. With boundary conditions

$$F(0) = F'(0) = F'(\infty) = \Theta(0) - \Theta_w = \Theta(\infty) - 1 = 0 \tag{23}$$

where Θ_W is the wall-to-ambient temperature ratio, these equations allow us to reduce the problem to

$$[\Theta^\sigma (\frac{F'}{R})']' + \frac{3}{5} F (\frac{F'}{R})' - \frac{1}{5R} F'^2 + \frac{2}{5}(\eta G' - G) = 0 \tag{24}$$

$$(\Theta^\sigma \Theta')' + \frac{3}{5} Pr F \Theta' = 0 \tag{25}$$

$$G' + R - 1 = 0 \tag{26}$$

A numerical solution is employed to solve the base flow problem. The easiest way to achieve this was found to be using Chebfun [10] integration with the above boundary conditions. Resulting profiles are shown in Fig. 2 for a range of Θ_W.

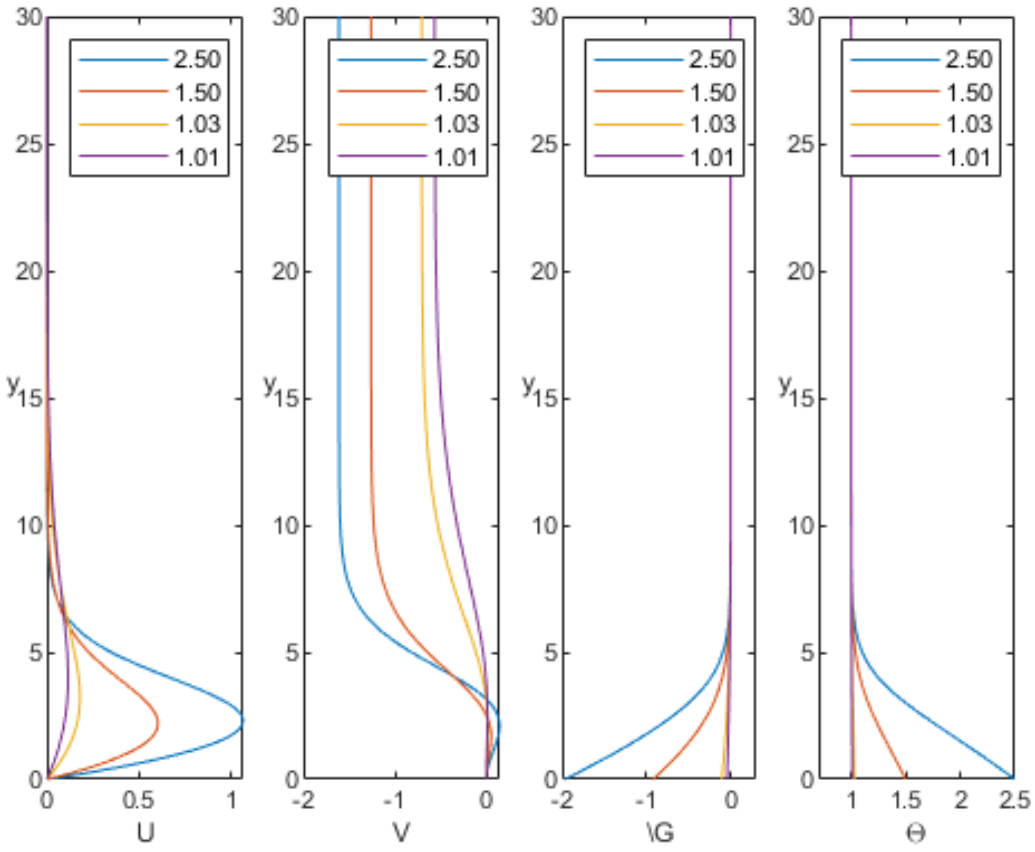

Figure 2: The self-similar base-flow solutions for different values of Θ_W

2.2 Linear stability analysis

The linear stability of the flow at $x^* = x_0^*$ is investigated by introducing the following the perturbed non-dimensional variables into Eq. (1) to (3) and Eq. (5) to (8):

$$\begin{aligned}
\frac{\mathbf{v}^*}{u_0^*} &= \bar{\mathbf{v}}(x/Gr, y) + \mathbf{v}(x, y, z, t) = (\bar{u}, \bar{v}, 0) + (u, v, w) \\
\frac{T^*}{T_\infty^*} &= \bar{\bar{T}}(x/Gr, y) + \theta(x, y, z, t) \\
\frac{\rho^*}{\rho_\infty^*} &= \bar{\rho}(x/Gr, y) + \rho(x, y, z, t) \\
\frac{\mu^*}{\mu_\infty^*} &= \bar{\mu}(x/Gr, y) + \mu(x, y, z, t) \\
\frac{p^*}{{\rho_\infty}^* u_0^{*2}} &= p(x, y, z, t)
\end{aligned} \tag{27}$$

and

$$x = \frac{x^* - x_0^*}{\delta_0^*}, y = \frac{y^*}{\delta_0^*}, z = \frac{z^*}{\delta_0^*}, t = \frac{t^*}{\delta_0^*/{u_0}^*}. \tag{28}$$

As a result, the linearized equations become:

$$\frac{\partial \rho}{\partial t} = -\bar{\rho}\nabla \cdot \mathbf{v} - \rho\nabla \cdot \bar{\mathbf{v}} - \mathbf{v} \cdot \nabla\bar{\rho} - \bar{\mathbf{v}} \cdot \nabla\rho, \tag{29}$$

$$\begin{aligned}
\bar{\rho}\frac{\partial \mathbf{v}}{\partial t} =& -\bar{\rho}\bar{\mathbf{v}} \cdot \nabla\mathbf{v} - \bar{\rho}\mathbf{v} \cdot \nabla\bar{\mathbf{v}} - \rho\bar{\mathbf{v}} \cdot \nabla\bar{\mathbf{v}} - \nabla p \\
& - \frac{1}{Gr}\rho\mathbf{e_y} + \frac{1}{Gr}\nabla \cdot [\bar{\mu}(\nabla\mathbf{v} + \nabla\mathbf{v}^T) + \mu(\nabla\bar{\mathbf{v}} + \nabla\bar{\mathbf{v}}^T)],
\end{aligned} \tag{30}$$

$$\begin{aligned}
\bar{\rho}\frac{\partial \theta}{\partial t} =& -\bar{\rho}\bar{\mathbf{v}} \cdot \nabla\theta - \bar{\rho}\mathbf{v} \cdot \nabla\bar{T} - \rho\bar{\mathbf{v}} \cdot \nabla\bar{T} \\
& - \frac{1}{Gr}\frac{1}{Pr}\nabla \cdot [\bar{\mu}\nabla\theta + \mu\nabla\bar{T}],
\end{aligned} \tag{31}$$

and

$$\rho = -\bar{T}^{-2}\theta, \mu = \sigma\bar{T}^{\sigma-1}\theta, \tag{32}$$

Based on the results of the self-similar velocity and temperature profiles, the base profiles then become with new notations:

$$\bar{u} = \bar{U}, \bar{v} = Gr^{-1}\bar{V}, \bar{T} = \frac{1}{\bar{\rho}}, \bar{T} = \bar{\mu}^{1/\delta}, D = \frac{\partial}{\partial_y} \tag{33}$$

using rescaled coordinates according to Eq. (28).

A reminder [6] is needed here that we assumed the slenderness of the flow previously. Hence the inverse of Gr, $\epsilon : Gr^{-1}$, is relatively small for the nearly parallel stability analysis used here. To impose this locally non-parallel flow assumption, some of the non-parallel terms of the base flow will be included in the stability equations. So only using terms up to $O(\epsilon^0)$ is not enough since they only describe the inviscid instability of strictly parallel flow. Thus, we decide to include terms up to $O(\epsilon^1)$ for the present work. Terms of $O(\epsilon^2)$ and higher are ignored.

$$\begin{aligned} \epsilon &: Gr^{-1} \\ O(\epsilon^0) &: \bar{U}, D\bar{U}, D^2\bar{U}, \\ &: \bar{T}, D\bar{T}, D^2\bar{T}, \\ O(\epsilon^1) &: \bar{V}, D\bar{V}, \\ &: \frac{\partial \bar{U}}{\partial x}, \frac{\partial \bar{T}}{\partial x}, \frac{\partial \bar{\rho}}{\partial x}, \\ O(\epsilon^2) &: \frac{\partial \bar{V}}{\partial x}, etc. \end{aligned} \tag{34}$$

Appendix A shows the simplified equations used for the numerical solution for the following normal-mode perturbations,

$$(p, u, v, w, \rho, \mu, \theta) = (\hat{p}(y), \hat{u}(y), i\hat{v}(y), \hat{w}(y), \hat{\rho}(y), \hat{\mu}(y), \hat{\theta}(y))e^{i(kx+lz-\omega t)} \tag{35}$$

where $\omega = \omega_r + i\omega_i$ contains both the frequency ω_r and the growth rate ω_i and k and l are the dimensionless streamwise and spanwise wave numbers.

3 Vortex instability

3.1 The simplified eigenvalue problem

We first study the appearance of the streamwise Görtler-like vortex rolls, known to be more prominent for cases with Boussinesq approximation. Following the linear stability analysis setup from the previous section, the eigenvalue problem can be simplified to make the calculations easier. It can be investigated by setting k = 0 in the normal-mode ansatz (Eq. (24)) and then constructed in the standard form $Af = \omega Bf$ with $f = (\hat{p}(y), \hat{u}(y), i\hat{v}(y), \hat{w}(y), \hat{\theta}(y))$. This equation is result from Eq. (35) where the $\hat{\rho}$ and $\hat{\mu}$ terms are expressed in terms of $\hat{\theta}$. In this particular case, an additional step can be taken to make the task even simpler. Chen et al. [11] proved the validity of the principle of exchange of stabilities for this type of instabilities, so it is in fact safe for us to believe that in the full eigenvalue spectrum, the eigenvalue with the largest growth rate ω_i has a corresponding zero real-part frequency ω_r. As a result, we can set ω equal to zero in addition to k in the simplified stability equations for the the critical conditions of vortex instability. However, this extra step was not taken during the numerical process. This allows us to keep the codes consistent with the one used for the wave modes.

3.2 Critical neutral stability curves

The above eigenvalue problem was then solved numerically so that we can determine the critical value Gr shown in Fig. 3. The top figure corresponds to the variation of Gr against l for different Θ_W. It can be seen that for each neutral curve, it reaches a minimum value Gr_m at a certain wave number l. This minimum determines the wave length with wave number l_m of the most unstable mode along with the downstream location $x_m^* = (Gr_m^5 {\nu_\infty}^2/g)^{\frac{1}{3}}$ at which the vortices begin to develop.

With these results, the variation of Gr_m and l_m for the most unstable mode is plotted as a function of Θ_W at the bottom as well. We can clearly conclude from the plots that increasing the wall-to-ambient temperature ratio Θ_W decreases the associated critical Grashof number and has a

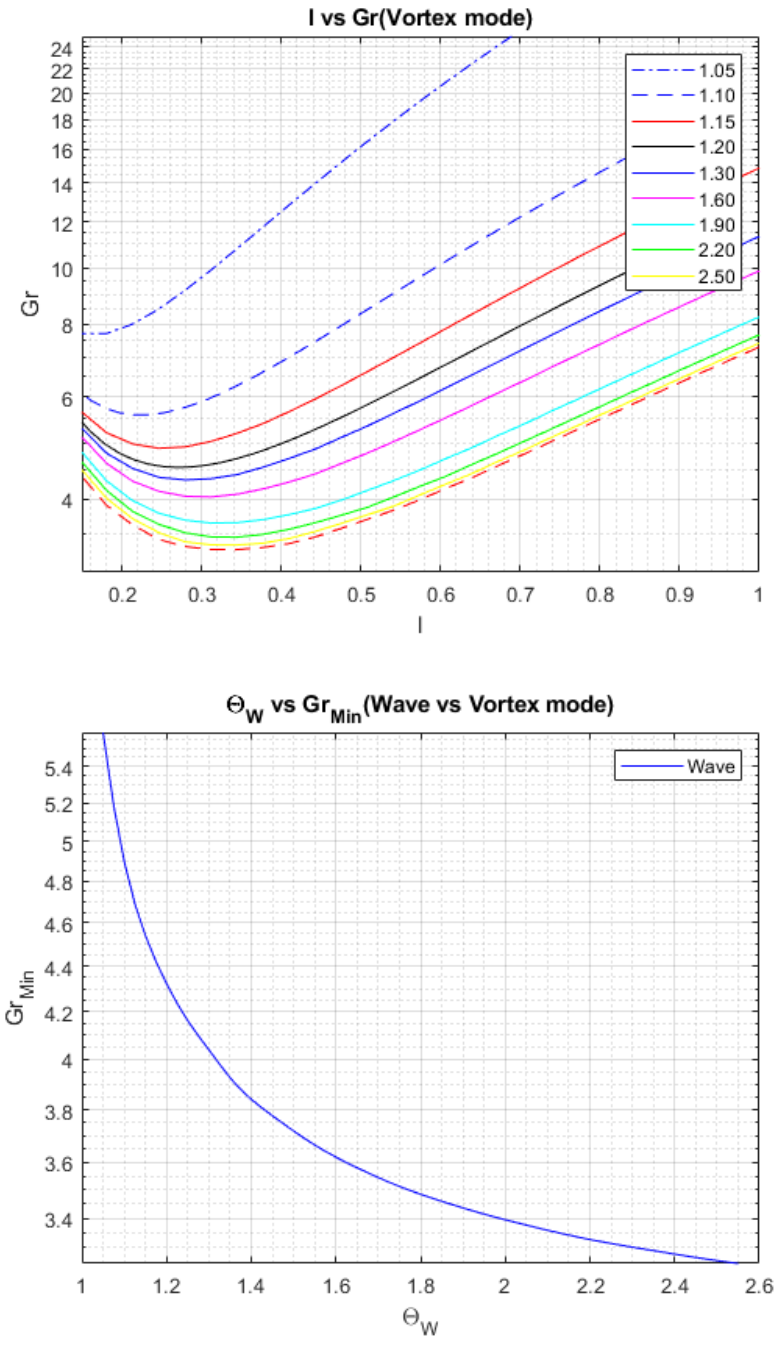

Figure 3: Results of the non-Boussinesq analysis of the vortex instability, including curves of neutral stability along the spanwise wave number l of different Θ_W(top) and critical Grashof number along the various temperature ratio Θ_W(bottom).

destabilizing effect on the flow. The departure of the critical Gr_m and l_m with higher Θ_W from when $\Theta_W - 1 \ll 1$ is also evident.

4 Wave instability

4.1 The simplified eigenvalue problem

As for the vortex mode, the eigenvalue problem for wave mode is simplified with a similar approach. However, unlike the vortex mode, the previous statement that in the full eigenvalue spectrum, the eigenvalue with the largest growth rate ω_i has a corresponding zero frequency ω_r does not hold true anymore and the condition $\omega = 0$ ceases to be valid. The wave number $l = 0$ becomes the only simplification can be employed and during the numerical solving process. All the equations are retained and the same standard form $Af = \omega Bf$ with $A$and B being linear differential operators is used for the sake of consistency. According to the existing literature [14,20], it is worth mentioning that even though a spatial stability analysis is recommended in terms of accuracy, a simpler temporal stability analysis is sufficient to determine the curves of neutral stability since we are only focusing on the the determination of the curves of neutral stability, associated with both the wave number k and the frequency ω.

4.2 Critical neutral stability curves

The above eigenvalue problem was solved numerically as well to determine the critical value Gr investigating the conditions of neutral stability for a given wall-to-ambient temperature ratio Θ_W, which defines the base flow, and a given streamwise wave number k. Fig. (4) shows the results obtained by integrating numerically the eigenvalue problem for the wave instability. Very similar to the vortex instability, increasing the wall-to-ambient temperature ratio tends to destabilize the flow. The departure observed previously is seen here as well, reinforcing the importance of non-Boussinesq effects for wave instability.

5 Comparison

For a more thorough understanding of the flow, an examination of the obtained results is

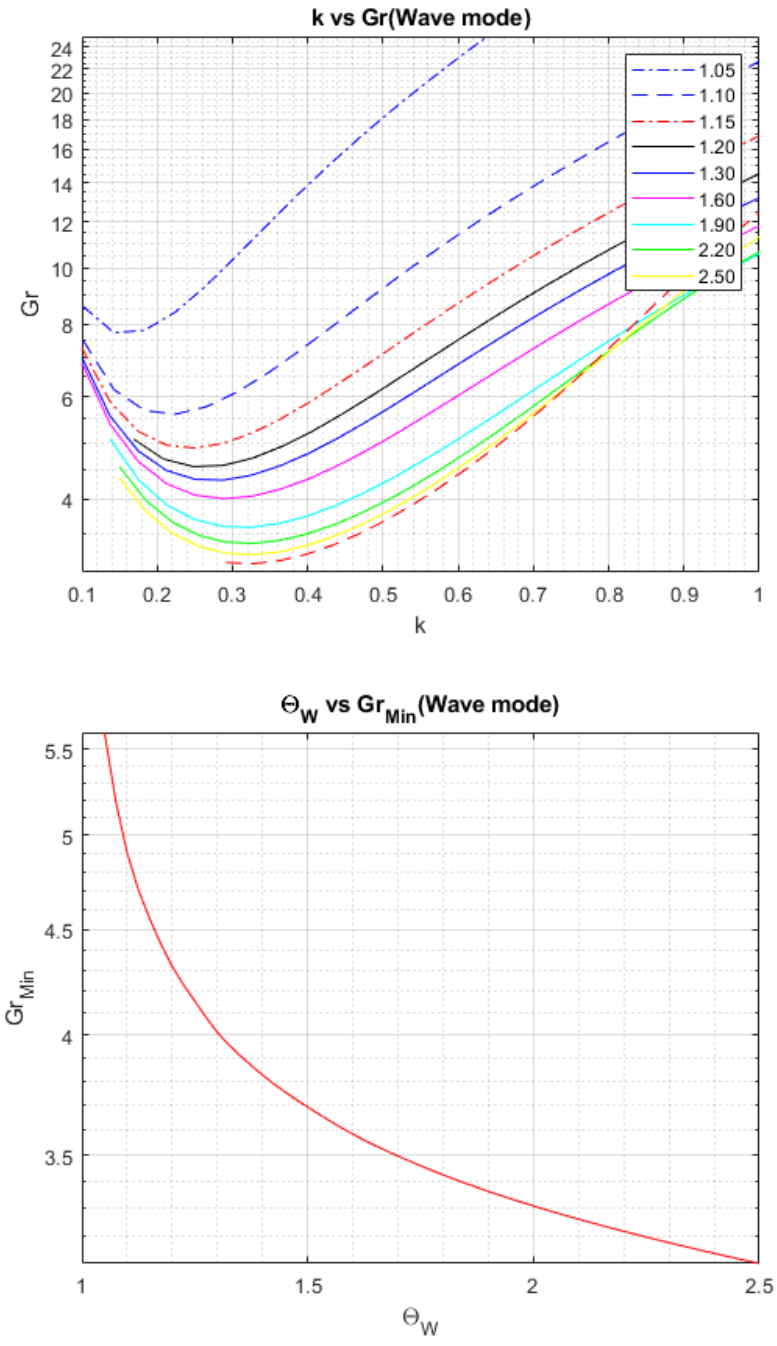

Figure 4: Results of the non-Boussinesq analysis of the vortex instability, including curves of neutral stability along the streamwise wave number k of different Θ_W(left) and critical Grashof number along the various temperature ratio Θ_W(right).

deemed to be necessary.

5.1 Results from the present study

We start by comparing our own vortex and wave modes instabilities results. As stated in sections 3 and 4, the eigenvalue problem was solved numerically to determine the critical value Gr for a range of wall-to-ambient temperature ratio Θ_W along different wave numbers. A similar setup of the standard form $Af = \omega Bf$ is used for both cases to ensure consistency. The minimum Gr of each neutral curve and the associated Θ_W is then plotted in Fig. (5) respectively. Here in

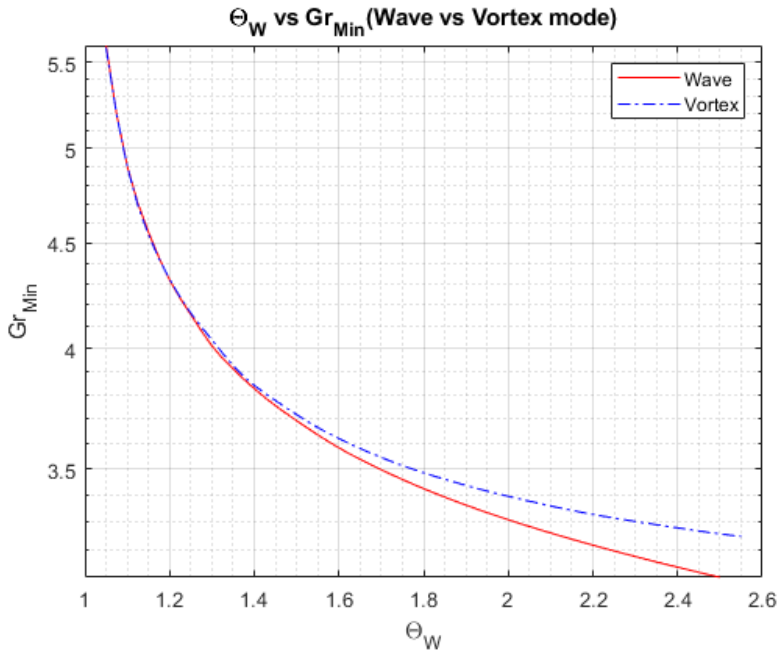

Figure 5: Curves of Θ_W against critical Grashof number for both vortex and wave modes.

Fig. (5), the two figures on the bottom from Fig. (3) and (4) are combined to see the effect of the various wall-to-ambient temperature ratios on both instability modes.

It is convenient for us to divide this figure into three sections: the low Θ_W section, the transition section and the high Θ_W a.k.a. the non-Boussinesq section.

The first section is the low Θ_W section shown in Fig. (6) and Fig. (7). This section should be categorized as the section when $\Theta_W - 1 \ll 1$. We can clearly see the similarity of the critical Grashof number for both the wave and vortex mode results. However, after enhancing the figures, it is worth noting that the vortex critical Gr is still slightly smaller than the wave critical Gr indicating that the vortex mode is being more dominant for a horizontal plate with low Θ_W value.

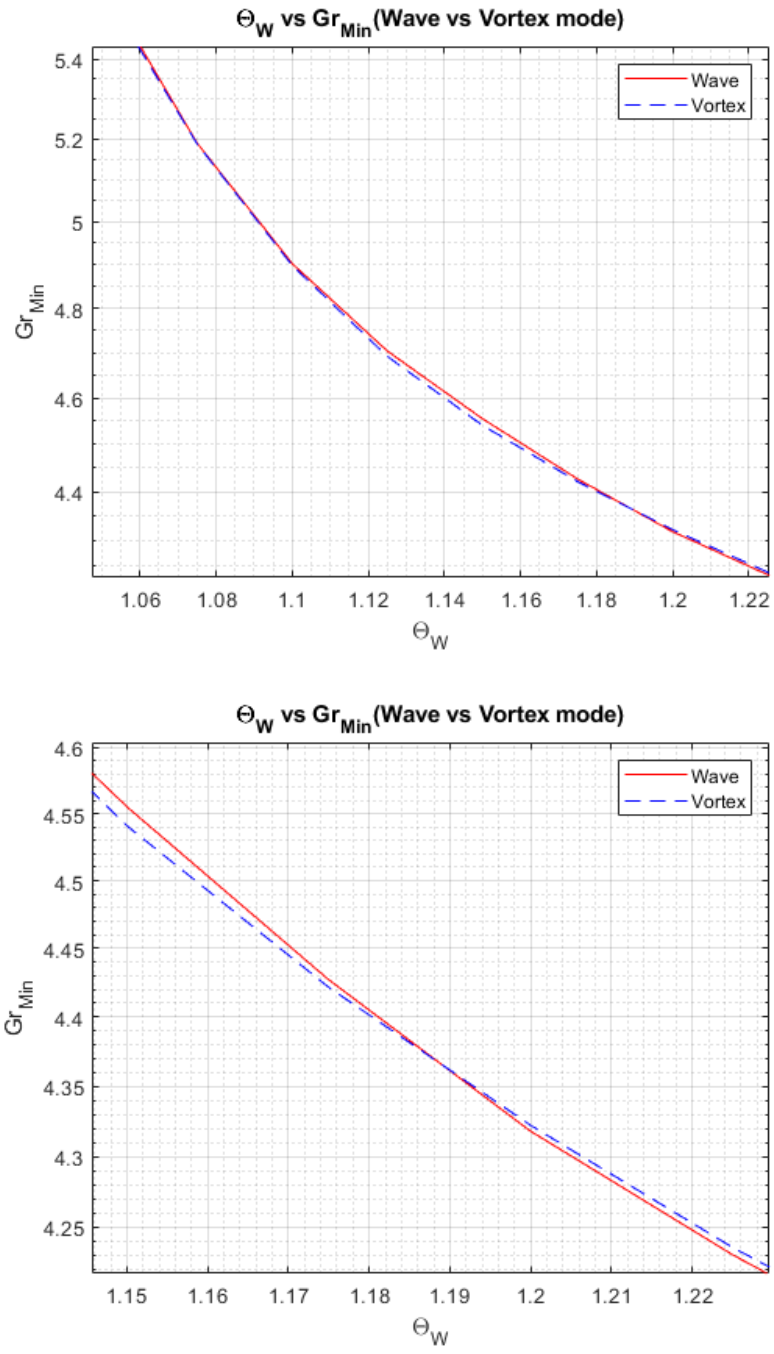

Figure 6: Magnified curves of Θ_W against critical Grashof number for both vortex and wave modes—low Θ_W region(left) and transition region(right).

The second section is the transition section. The smaller critical Grashof number at a given wall-to-ambient temperature ratio slowly changes from the one obtained from the vortex mode to

the one from the wave mode, shown in Fig. (6)(bottom) as Θ_W increases. In the magnified plot, it is noticed that such transaction happens at a Θ_W around 1.19. This is very close to the threshold where we define the flow as transitioning from being valid for Boussinesq approximation to non-Boussinesq approximation.

The third section would then be the high Θ_W section where the non-Boussinesq approximation should be employed,shown in Fig. (5) and (8) It is evident that the wave mode curve contains the smallest critical Grashof numbers whereas the gap between the vortex and wave mode Gr increases as Θ_W increases.

Based solely on these observations, it is clear for a non-Boussinesq natural-convection flow over a horizontal hot plate, as Θ_W increases, the susceptibility of the flow to the vortex mode of instability decreases while the wave mode instability becomes much more dominant, and this holds especially true when Θ_W is out of the Boussinesq approximation range.

5.2 Comparison with results from existing literature

We now compare the present results with results from existing literature. Three papers are mainly compared for a better understanding of the present instability analysis.

5.2.1 Inclined plate with non-Boussinesq approximation

Rajamanickam et al. [6] examined the non-Boussinesq effect on an inclined plate and their corresponding formulation is based on these conditions. According to [6], with a fixed inclination angle, the increasing of Θ_W decreases the associated critical Grashof number which is more pronounced for the wave mode indicating the instability may switch from vortex mode to wave mode as the plate temperature increases.

This behavior is in consistent with what we observed from the present work for horizontal hot plate. Essentially, we can consider our horizontal plate as a unique situation where the given inclination angle is fixed at 90 degrees according to [6]'s convention when the angle is set from the vertical plane. One aspect should be kept in mind is that Rajamanickam's [6] formulations is

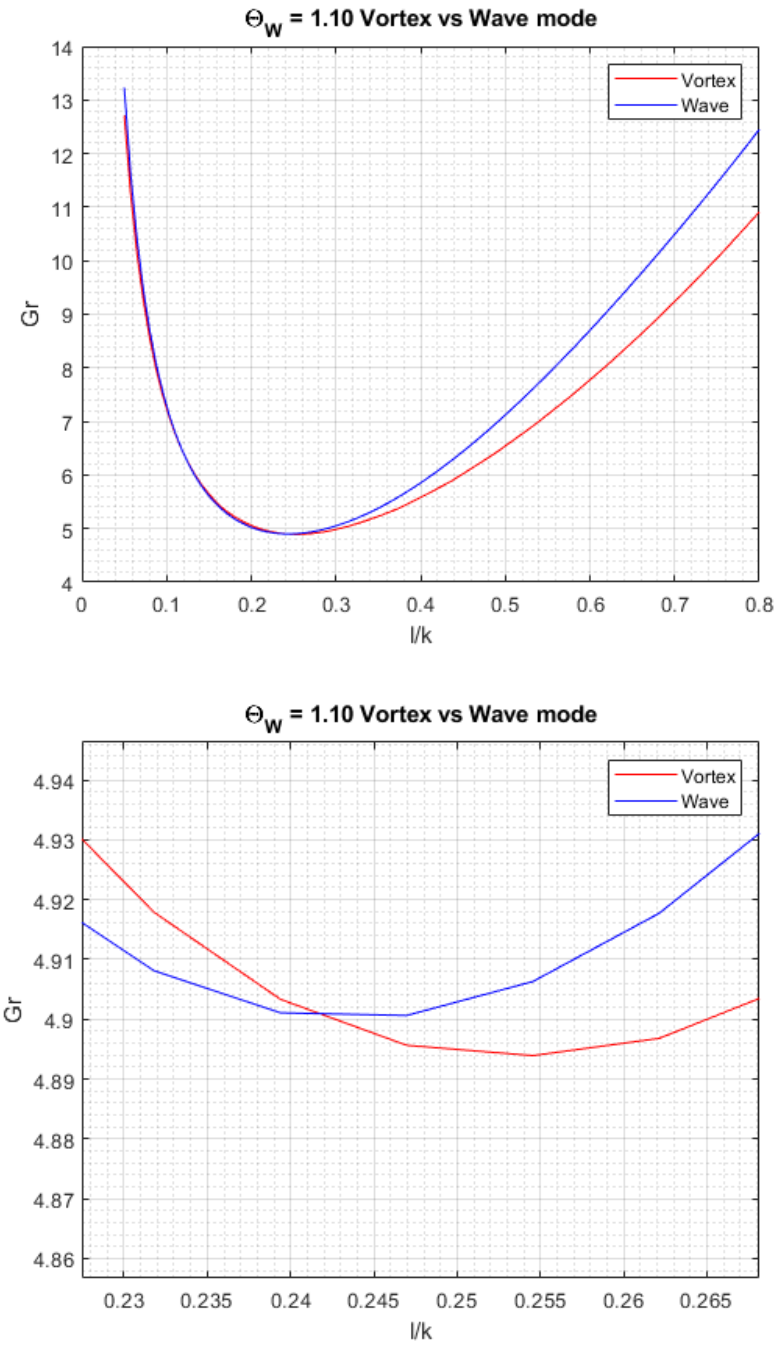

Figure 7: Curves of wave number k/l against critical Grashof number for both vortex and wave modes for low Θ_W—regular(left) and magnified(right)..

not suitable for completely horizontal plate due to the derivation from inclined conditions. But a prediction can still be made and as we learned from the previous subsections, the horizontal hot plate based on our work indeed exhibits such behavior where the wave mode instability becomes

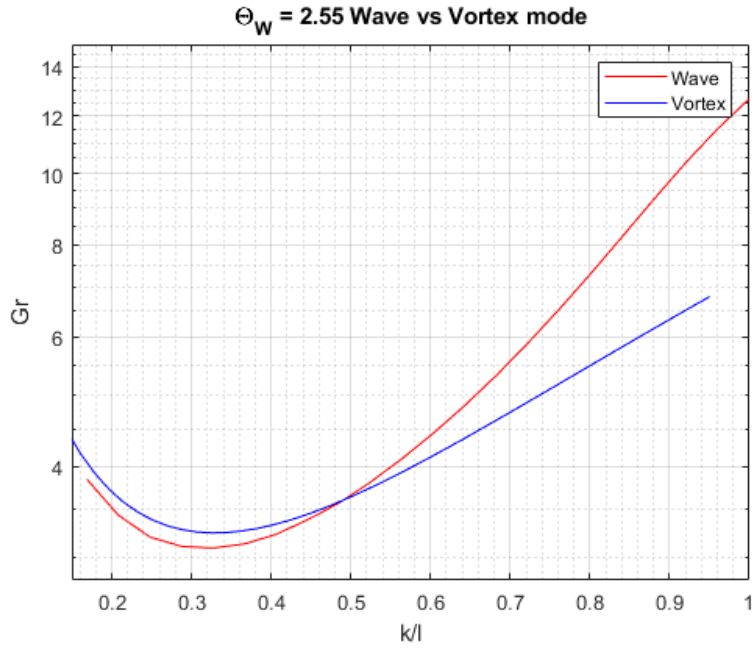

Figure 8: Curves of wave number k/l against critical Grashof number for both vortex and wave modes for high Θ_W

more prominent than the vortex mode one when Θ_W increases.

However, one factor needs to be noted is that the Gr used in [6], similar to our definition, appears to be larger than our results even for high Θ_W. This discrepancy is very important and will be discussed during the concluding remarks.

5.2.2 Horizontal plate with Boussinesq approximation

The two papers from Chen et al. [7] [8] are used as comparison to study the departures from the Boussinesq approximation

Chen et al. [7] [8] showed the Boussinesq effect on a horizontal plate and their formulation is based on this approximation. A Grashof number is defined as follows for both vortex and wave mode,

$$Gr_{chen} = g\beta(T_w - T_\infty)x^3/\nu^2. \tag{36}$$

For a horizontal plate a critical Gr number of 340 for vortex mode and a critical Gr number of 510

for wave mode are obtained from [7] [8]. With these two values, a prediction derived by extending the Boussinesq approximation using high Θ_W employing the following equation can be made.

$$Gr = (\frac{Gr_{chen}}{\beta(T_w - T_\infty)})^{\frac{2}{5}} \tag{37}$$

Two coefficients of thermal expansion β are choosen with $\beta_w = 1/T_w$ and $\beta_\infty = 1/T_\infty$. The vortex mode plot is then shown in Fig. (9) and the wave mode plot is shown in Fig. (10).

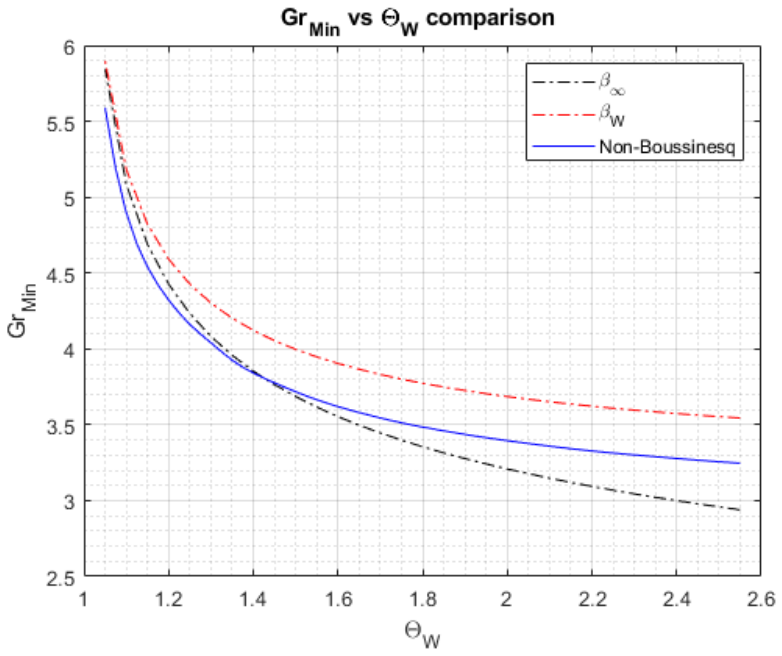

Figure 9: Curves of critical Gr with different Θ_W from present study (solid curve) and from the Boussinesq predictions obtained by scaling the value given in [7] for the vortex mode

For the vortex mode, the curve representing results from present work lies between the two Boussinesq predictions, with the thermal expansion $\beta_\infty = 1/T_\infty$ based on the ambient temperature being a better fit while for the wave mode, we can see that the curve representing results from present work lies below both Boussinesq predictions regardless of value of the thermal expansion. It is safe to say that an extension from the Boussinesq approximation can be used to predict situations even when $\Theta_W - 1 \sim 1$. However, since the wave mode becomes more prominent for high

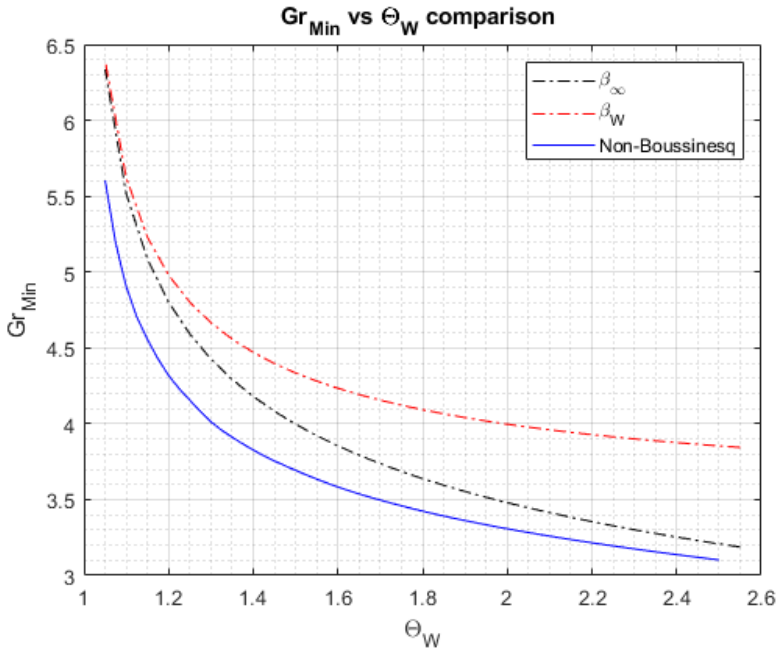

Figure 10: Curves of critical Gr with different Θ_W from present study (solid curve) and from the Boussinesq predictions obtained by scaling the value given in [8] for wave mode

Θ_W and the solid curve in Fig. (10) lies below the predicted curves, such an extension becomes less sufficient even with a very small difference in value and our non-Boussinesq calculation needs to be considered instead. Again, one factor needs to be noted is that the critical Gr for high Θ_W here stops being $\gg 1$ and this will be discussed during the concluding remarks as well.

6 Conclusion

The present work fills the void for the study of a flow that develops over a horizontal hot plate among previous experimental and theoretical researches. Both instability modes: vortex—Görtler-like streamwise vortices and wave—spanwise traveling waves are examined. It is shown that the non-Boussinesq effect indeed plays an important role on the dominance of the two instability modes. The results provide predictions of critical Grashof numbers for both vortex and wave modes of instability and their associated wave numbers, and show that as Θ_W increases, the susceptibility of the flow to the vortex mode of instability indeed decreases while the wave mode instability becomes more prominent. Based on comparisons with existing literature, unlike the

inclined plate, the horizontal plate is only moderately affected by non-Boussinesq conditions for both vortex and wave instabilities even though it is still found that such conditions promotes wave instabilities slightly more.

However, one significant flaw of the present work is that the resulting critical Gr number fails to meet the slenderness requirement for boundary-layer region as Θ_W increases. As shown in section 5, the resulting critical Gr when $\Theta_W = 2.50$ is around 3.0 and the order of magnitude of that value contradicts with our assumption. The promise of having a large Gr as indicated in Eq. (16) is crucial to maintain the validity of our work. As a result, further improvement regarding the setup of the problem is warranted.

For instance, a non-local parabolic stability problem could proved to be useful in this case. Inspired by [6], a global stability analysis in which the instabilities are considered as two dimensional temporal Fourier modes, is worth considering as well. The core of this approach is that it does not require the flow to be slender and then the Navier-Stokes region could perhaps be studied.

A Appendix

The simplified stability equations are shown below with $\hat{\rho} = -\bar{\Theta}^{-2}\hat{\theta}$ and $\hat{\mu} = \sigma\hat{\Theta}^{\sigma-1}\hat{\theta}$,

$$(0)\hat{p} + (ik\bar{\rho} + \partial_x\bar{\rho})\hat{u} + (il\bar{\rho})\hat{v} + (i\bar{\rho}D + iD\bar{\rho})\hat{w} + \tag{38}$$
$$(\partial_x\bar{U} + ik\bar{U} + Gr^{-1}\bar{W}D + Gr^{-1}D\bar{W})\hat{\rho} + (0)\hat{\mu} + (0)\hat{\theta} = \omega(i)\hat{\rho}$$

$$(ik)\hat{p} + (ik\bar{\rho}\bar{U} + \rho\partial_x\bar{U} + Gr^{-1}\bar{\rho}\bar{W}D - Gr^{-1}[\bar{\mu}(D^2 - 2k^2 - l^2) + D\mu D])\hat{u} + \tag{39}$$
$$(Gr^{-1}\bar{\mu}kl)\hat{v} + (i\bar{\rho}D\bar{U} + Gr^{-1}[kD\bar{\mu} + k\bar{\mu}D])\hat{w} +$$
$$(\bar{U}\partial_x\bar{U} + Gr^{-1}\bar{W}D\bar{U})\hat{\rho} + (-Gr^{-1}[\partial_z z\bar{U} + D\bar{U}D])\hat{\mu} + (0)\hat{\theta} = \omega(i\rho)\hat{u}$$

$$(il)\hat{p} + (Gr^{-1}\bar{\mu}kl)\hat{u} + \tag{40}$$
$$(ik\bar{\rho}\bar{U} + Gr^{-1}\bar{\rho}\bar{W}D - Gr^{-1}[\bar{\mu}(D^2 - k^2 - l^2) + D\mu D])\hat{v} +$$
$$(Gr^{-1}[lD\bar{\mu} + l\bar{\mu}D])\hat{w} + (0)\hat{\rho} + (0)\hat{\mu} + (0)\hat{\theta} = \omega(i\rho)\hat{v}$$

$$(D)\hat{p} + (-Gr^{-1}ik\bar{\mu}D)\hat{u} + (-Gr^{-1}il\bar{\mu}D)\hat{v} + \tag{41}$$
$$(-\bar{\rho}\bar{U}k + i\bar{\rho}Gr^{-1}\bar{W}D + i\bar{\rho}Gr^{-1}D\bar{W} - Gr^{-1}[i\bar{\mu}(2D^2 - k^2 - l^2) + i2D\mu D])\hat{w} +$$
$$(1)\hat{\rho} + (-Gr^{-1}ikD\bar{U})\hat{\mu} + (0)\hat{\theta} = \omega(-\bar{\rho})\hat{w}$$

$$(0)\hat{p} + (\rho\partial_x\bar{T})\hat{u} + (0)\hat{v} + (i\bar{\rho}D\bar{T})\hat{w} + \tag{42}$$
$$(\bar{U}\partial_x\bar{T} + Gr^{-1}\bar{W}D\bar{T})\hat{\rho} + (-Gr^{-1}Pr^{-1}[D\bar{T}D + \partial_z z\bar{T}])\hat{\mu} +$$
$$(ik\bar{\rho}\bar{U} + Gr^{-1}\bar{\rho}\bar{W}D - Gr^{-1}Pr^{-1}[\bar{\mu}(D^2 - k^2 - l^2) + D\mu D])\hat{\theta} = \omega(i\bar{\rho})\hat{\theta}$$

and boundary conditions,

$$\hat{u} = \hat{v} = \hat{w} = \hat{\theta} = 0 \qquad \text{at } y = 0 \tag{43}$$
$$\hat{u} = \hat{v} = \hat{w} = \hat{\theta} = \hat{p} = 0 \qquad \text{as } y \to \infty$$

The equations are prepared for the linear differential operators$A$and B used in the standard form $Af = \omega Bf$ with f in the form of Eq. (44)

One important note is that all terms along the y- and z- directions are interchanged with each other for coding purpose. Eqa. (35) is converted and takes the following form.

$$(p, u, v, w, \rho, \mu, \theta) = (\hat{p}(z), \hat{u}(z), \hat{v}(z), i\hat{w}(z), \hat{\rho}(z), \hat{\mu}(z), \hat{\theta}(z))e^{i(kx+ly-\omega t)} \tag{44}$$

References

[1] Massimo Corcione. Heat transfer correlations for free convection from upward-facing horizontal rectangular surfaces. *WSEAS Transactions on Heat and Mass Transfer*, 2(3):48–60, 2007.

[2] Ernst Schmidt and Wilhelm Beckmann. Das temperatur-und geschwindigkeitsfeld vor einer wärme abgebenden senkrechten platte bei natürlicher konvektion. *Technische Mechanik und Thermodynamik*, 1(11):391–406, 1930.

[3] EM Sparrow and RB Husar. Longitudinal vortices in natural convection flow on inclined plates. *Journal of Fluid Mechanics*, 37(2):251–255, 1969.

[4] SE Haaland and EM Sparrow. Vortex instability of natural convection flow on inclined surfaces. *International Journal of Heat and Mass Transfer*, 16(12):2355–2367, 1973.

[5] SE Haaland and EM Sparrow. Wave instability of natural convection on inclined surfaces accounting for nonparallelism of the basic flow. *Journal of Heat Transfer*, 95(3):405–407, 1973.

[6] Prabakaran Rajamanickam, Wilfried Coenen, and Antonio L Sánchez. Non-boussinesq stability analysis of natural-convection gaseous flow on inclined hot plates. *International Journal of Heat and Mass Transfer*, 109:949–957, 2017.

[7] TS Chen and Keh-Lih Tzuoo. Vortex instability of free convection flow over horizontal and inclined surfaces. *Journal of Heat Transfer*, 104(4):637–643, 1982.

[8] Keh-Lih Tzuoo, TS Chen, and Bassem F Armaly. Wave instability of natural convection flow on inclined surfaces. *Journal of heat transfer*, 107(1):107–111, 1985.

[9] JF Clarke and N Riley. Natural convection induced in a gas by the presence of a hot porous horizontal surface. *The Quarterly Journal of Mechanics and Applied Mathematics*, 28(4):373–396, 1975.

[10] T. A. Driscoll, N. Hale, and L. N. Trefethen. Chebfun. 2014.

[11] CC Chen, A Labhabi, H-C Chang, and RE Kelly. Spanwise pairing of finite-amplitude longitudinal vortex rolls in inclined free-convection boundary layers. *Journal of Fluid Mechanics*, 231:73–111, 1991.